Modulated Model Predictive Control for Modular Multilevel AC/AC Converter

He, Zhixing; Guo, Peng; Shuai, Zhikang; Xu, Qianming; Luo, An; Guerrero, Josep M.

Published in:
IEEE Transactions on Power Electronics

DOI (link to publication from Publisher):
10.1109/TPEL.2019.2895224

Publication date:
2019

Document Version
Accepted author manuscript, peer reviewed version

Modulated Model Predictive Control for Modular Multilevel AC/AC Converter

Zhixing He, *Member, IEEE*, Peng Guo, *Student Member, IEEE*, Zhikang Shuai, *Member, IEEE*, Qianming Xu, *Member, IEEE*, An Luo, *Senior Member, IEEE* and Josep M. Guerrero, *Fellow, IEEE*

***Abstract*—Modular multilevel converter (MMC) is very popular in high power applications due to its attractive characteristics. The full bridge-based MMC featuring three-phase to single-phase direct AC/AC conversion is a potential solution for ac power supply (ACPS). In this paper, new modulated model predictive control (MMPC) methods are proposed for MMC-ACPS to improve the steady state multi-objective current tracking performance. In the proposed methods, modulated vectors sequence is employed, output voltage levels of upper and lower arms are combined and represented by vectors in the current increments plane firstly. Then, the plane is divided into eight sectors according to the predictive tracking errors of input current and circulating current. After determining sectors, a modulated vector sequence, consisting of one zero vector and two active vectors, is selected to eliminate these current tracking errors simultaneously at the end of each control period. Duty cycles of the three selected vectors are calculated based on the principle of multiple current tracking errors minimization. Optimized vector selection approaches are illustrated in detail for the proposed MMPC. Since only the adjacent nine vectors are utilized in the proposed methods, the calculation amount is suitable and the dv/dt of the output voltage is also limited. Finally, steady-state and dynamic performances of the proposed control methods are verified by experimental results.**

***Index Terms*—Modulated model predictive control, ac power supply, AC/AC conversion, modular multilevel converter.**

I. Introduction

Recently, the modular multilevel converters (MMC) which have characteristics of natural modular expansion, low switching frequency and high-efficiency [1]-[4], have gained extensive attentions and rapid developments in high voltage direct current (HVDC) systems, high power motor drives, energy storages, as well as advanced grid-connected and railway applications [5]-[8]. Compared with the half bridge based structure, the full bridge based MMC features direct three-phase to single phase AC/AC function because its submodule (SM) can output negative voltage [9]-[10]. From this perspective, MMC is an attractive topology for direct three-phase to single phase AC/AC power supply (ACPS).

Conventionally, the AC/AC converter can be classified into three subcategories including converter with dc-link storage, matrix converter, and hybrid matrix converter [11]. The most widely used AC/AC converter topology with dc-link storage is the two-level voltage source back-to-back converter. The AC/AC converter without any energy storage in the intermediate link is referred to as matrix converter (MC), which achieve the simultaneous amplitude and frequency transformation of AC/AC system. The AC/AC converter with combining the back-to-back converter and MC is called as hybrid MC. If the four-quadrant switches in MC are replaced by cascaded H-bridge with storage capacitor, the hybrid MC will possess the capability of the step up or step-down converter operation. In this opinion, the new AC/AC MMC firstly proposed in [1] can be regard as the hybrid MC. The topologies of single-phase to single-phase and the three-phase to single-phase AC/AC MMC are presented in [1]. Comparing with other AC/AC converters, the AC/AC MMC features a very consistent redundancy and can be expanded to different voltage and power level due to its modular structure. The three-phase to three-phase AC/AC MMC, namely the Modular Multilevel Matrix Converter (M3C), and its cascaded control method are introduced in [12]. A new three-phase AC/AC MMC with six branches in hexagonal configuration is proposed in [13]. The AC/AC MMC is employed to the induction heating molten steel application [14]. In the application of induction heater in the casting process, the power source is single-phase and it should supply low output frequency but high power. The conventional topology of induction heating power supply is comprised of multi-winding transformer, three-phase diode rectifiers and cascaded full bridges converter [14]. Each diode rectifier provides dc power to the dc side of each full bridge converter, the full bridges connected in series in the output side to provide high voltage single-phase ac power to the load. The conventional structure can easily achieve the AC/AC conversion from three-phase to single-phase, but the operating range of dc capacitors voltages is limited due to unidirectional power flow. Additionally, it will significantly increase the size and cost of the power supply because of the indispensable multi-winding transformer. Comparing to the conventional power supply, the MMC-ACPS can be connected to the high-voltage grid directly without the bulky multi-winding transformer. Further, the MMC-ACPS has the capacity of bidirectional

Manuscript received Apr 12, 2018; revised July 10, 2018; revised Oct 11; accepted Jan 13, 2019. This work was supported by the National Natural Science Foundation of China under Grant 51807057; National Key R&D Program of China under Grant 2016YFE0123900.

Z. He, P. Guo, Z. Shuai, Q. Xu and A. Luo are with the College of Electrical and Information Engineering, Hunan University, Changsha 410082, China (e-mail: hezhixingmail@163.com; pengguo92@hnu.edu.cn; szk@hnu.edu.cn; hnuxqm@foxmail.com; an_luo@126.com).

J. M. Guerrero is with the Department of Energy Technology, Aalborg University, 9220 Aalborg East, Denmark (e-mail: joz@et.aau.dk).

Color versions of one or more of the figures in this paper are available online at http://ieeexplore.ieee.org.

Digital Object Identifier xx.xxxx/TPEL.2019.xxxxxxx

power flow, better current control performance and it can achieve unit power factor in the input side. For these reasons, the three-phase to single-phase AC/AC MMC topology is studied. While, the M3C in [12] and the hexverter in [13] are more suitable for three-phase to three-phase conversion, then the full bridge based MMC is selected for the three-phase to single phase AC/AC conversion in this paper. In fact, the three-phase to single phase AC/AC MMC can be regard as a special topology of the M3C because those topologies are all built by the full bridge based modular multilevel branches.

One of the main technical challenges associated with MMC-ACPS is the current control. MMC has multiple current control objectives, such as input currents and circulating current. Furthermore, the currents inside MMC-ACPS contain two different frequency components since the input current frequency and output current frequency are different, which introduces extra control challenges. Over the past few years, various current control methods have been proposed for MMC, including the proportional-integral (PI) control method based on synchronous frame, proportional resonant control (PR), repetitive control, deadbeat control and so on [14]-[19]. PI controller is a good method to regulate dc component, but significant tracking errors might occur for ac currents. As for PR controller, zero error tracking only occurs at the resonant frequency. Deadbeat control is quite simple because its control parameters can be chosen according to the discrete-domain states equations, and the current tracking errors are reduced by amplifying the errors between the current references and the sampled values in the deadbeat control. Recently, the finite control set model predictive control (FCS-MPC) method gained extensive attentions and has been applied to a wide range of power converters [20]-[24]. In FCS-MPC, the control objectives are evaluated by a cost function, the control set which minimizes the cost function is chosen as the optimal one and applied in the next control period. FCS-MPC is a nonlinear optimization control method and has the characteristics of good control effect and dynamic performance. This method has been used to minimize the circulating currents of MMC in [25] and [26]. Experimental evaluation of MPC for MMC is presented in [27]. MPC is compared with the cascaded control method in [28]. In [29], a predictive approach is proposed to minimize the input, output, and circulating current errors and to balance the dc voltages of the single-phase AC/AC MMC.

However, calculation amount is the main barrier when MPC is applied to MMC [30]-[33]. In conventional FCS-MPC, cost function is evaluated for all possible switch state combinations [22]-[25]. As the voltage level increased, the number of possible switch states combinations increases geometrically, which causes large calculation amount. To reduce the computation burden, a MPC method with reduced number of considered states is proposed in [30] to control the ac-side currents along with circulating currents and SM capacitor voltages, three different cost functions are defined to select the best switching state. In [31], an indirect strategy is proposed to reduce the calculation amount by determining the number of inserted or bypassed SM within each arm, the number of switching options can be reduced further when only the neighboring index values with respect to their previously applied values were considered. A dual-stage MPC approach to solve the issues of computational burden and unwanted switching is proposed in [32], control objectives are evaluated corresponding to the redundancies of voltage vectors and SMs respectively. Switching state grouping based MPC, voltage level based MPC and rolling optimization process simplifying based MPC are also investigated in [33] to [35].

The other issue of FCS-MPC is the large steady-state current tracking errors and current ripples because only one optimal switching state is applied during the entire sampling period. Hence, an increased control frequency are always required to achieve high control performance comparable to the modulation-based methods [36]-[38], which results in extra computational burden. To deal with this problem, two improved approaches combining multiple vectors with variable durations have been proposed for two-level converters in [36] and [37]. Linear combination of two different output levels is also proposed to improve the single current control performance of cascaded H-bridge converters in [38] and [39]. While, multiple current control objectives should be achieved simultaneously for MMC-ACPS. A new modulated model predictive control method is proposed for MMC in VSC-HVDC systems in [40], while, only one extra SM is employed to control circulating current and the method is an independent-objective control strategy. While, for MMC-ACPS, the input current and output current are alternating currents and coupled, the multi-objective coordinative current tracking error eliminating is quite difficult.

In this paper, a MMPC approach is proposed for MMC-ACPS to improve the steady state multi-objective current control performance and reduce the computation burden. The proposed method incorporates several innovative ideas. Combinations of upper arm output voltage level and lower arm output voltage level are firstly represented by vectors in the current increments plane. With these vectors, eight sectors are also defined. Then, two MMPC approaches with different modulated vectors sequences are proposed to eliminate the input current and circulating current tracking errors simultaneously at the end of each control period. In the proposed methods, one zero vector and two optimal active vectors are selected for each sector, meanwhile, the duty cycles of these vectors are calculated in a very simple way according to the principle of multiple current tracking errors minimization. The rest of this paper is organized as follows. In section II, the mathematical model and capacitor voltage ripples of MMC-ACPS are introduced and derived. In section III, the proposed MMPC approach are presented in detail. Then, the control strategy of MMC-ACPS is shown in section IV, followed by the experimental results in Section V and conclusion in Section VI.

II. Mathematical Model and Capacitor Voltage Ripple

A. System structure and mathematical model

Fig.1 shows the circuit diagram of a three-phase to single-phase H-bridge MMC-ACPS. Each phase cluster has

This article has been accepted for publication in a future issue of this journal, but has not been fully edited. Content may change prior to final publication. Citation information: DOI 10.1109/TPEL.2019.2895224, IEEE Transactions on Power Electronics

two arms, each arm consists of *N*-series H-bridge SMs. In Fig. 1, u_{gx} (x = a, b, c) and i_{sx} are the grid voltages and input currents, i_{ux}, i_{lx} and u_{ux}, u_{lx} are the currents and output voltages of upper and lower arms. L, L_g and R are the arm inductance, grid side inductance and equivalent resistance, i_o and u_o are the output current and voltage. The midpoint of the output link is regard as neutral point for facilitation of the analysis [28] and [33]. MMC-ACPS can be used as the power source of induction heater, the induction heater works similar to single-phase transformer in the continuous casting process. More precisely, the induction heater can be simplified to a resistance-inductance load as shown in Fig. 1, R_L is the load resistance and L_L is the load inductance.

Applying the KVL and KCL, the mathematical model equations are obtained as follows

$$\begin{cases} \dfrac{u_o}{2} = u_{gx} + u_{ux} + L\dfrac{di_{ux}}{dt} + Ri_{ux} - L_g\dfrac{di_{sx}}{dt} \\ \dfrac{u_o}{2} = -u_{gx} + u_{lx} + L\dfrac{di_{lx}}{dt} + Ri_{lx} + L_g\dfrac{di_{sx}}{dt} \end{cases} \tag{1}$$

$$\begin{cases} i_{ux} = -\dfrac{i_{sx}}{2} + i_{cx} \\ i_{lx} = \dfrac{i_{sx}}{2} + i_{cx} \end{cases} \tag{2}$$

$$\begin{cases} i_o = -(i_{ca} + i_{cb} + i_{cc}) \\ u_o = L_L\dfrac{di_o}{dt} + R_L i_o \end{cases} \tag{3}$$

Where i_{cx} is the circulating current flowing through each phase cluster of MMC-ACPS. Combining (1) and (2), the dynamic equation of input current and circulating current in each phase can be expressed as

$$\begin{cases} \dfrac{di_{sx}}{dt} = -\dfrac{R}{\lambda_1 L}i_{sx} - \dfrac{1}{\lambda_1 L}u_{sx} + \dfrac{2}{\lambda_1 L}u_{gx} \\ \dfrac{di_{cx}}{dt} = -\dfrac{R}{L}i_{cx} - \dfrac{1}{2L}u_{cx} + \dfrac{1}{2L}u_o \end{cases} \tag{4}$$

Where u_{sx}=(u_{lx}-u_{ux}) and u_{cx}=(u_{lx}+u_{ux}) are the differential and common mode voltage of each phase cluster, $\lambda_1 L$=2L_g +L. Discretizing the continuous model with the control period T_s, the discrete-domain state space equation can be expressed as (5), where $i_{sx}(k+1)$, $i_{cx}(k+1)$ and $i_{sx}(k)$, $i_{cx}(k)$ are currents at the (k+1)th and the kth control period respectively, $u_{gx}(k)$ and $u_o(k)$ are the grid voltage and output voltage at the kth control period which can be regard as disturbances in the state space equation.

B. System structure and capacitor voltage ripple

MMC-ACPS is an attractive structure for power source of induction heater in continuous casting process, the frequency of

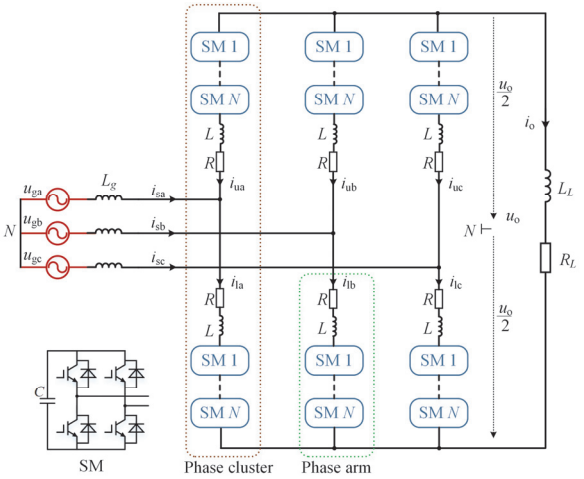

Fig. 1 Circuit diagram of the three-phase H-bridge MMC-ACPS.

output current ω_o is different with the one of grid side input current ω_g. When these different frequency current components flow through the capacitor of each SM, the voltage ripple becomes complicated. In this part, the capacitor voltage ripple is derived in the steady state and the effect caused by the voltage ripples on current control will discussed in the following.

Assuming that the SM capacitor voltages are well balanced at their reference values, using a-phase as an example, the average switching function S_{ua} and S_{la} of the SMs in the upper and lower arms can be expressed as

$$\begin{cases} S_{ua} = -\dfrac{1}{2}M_s\sin(\omega_g t) + \dfrac{1}{2}M_c\sin(\omega_o t + \theta_o) \\ S_{la} = \dfrac{1}{2}M_s\sin(\omega_g t) + \dfrac{1}{2}M_c\sin(\omega_o t + \theta_o) \end{cases} \tag{6}$$

Where M_s and M_c are the modulation indexes of the differential and common mode voltage, θ_o is the initial angle of common mode voltage. Arm currents are utilized in the voltage ripple analysis. Based on (2), the currents can be expressed as

$$\begin{cases} i_{ua} = -\dfrac{1}{2}I_s\sin(\omega_g t + \varphi_{ga}) + \dfrac{1}{3}I_o\sin(\omega_o t + \theta_o + \varphi_o) \\ i_{la} = \dfrac{1}{2}I_s\sin(\omega_g t + \varphi_{ga}) + \dfrac{1}{3}I_o\sin(\omega_o t + \theta_o + \varphi_o) \end{cases} \tag{7}$$

Where I_s and I_o are the amplitude of input current and output current, φ_{ga} and φ_o are the current angles. Note that the circulating current components which are utilized to balancing the capacitor voltages of SMs are neglected because these components are quite small comparing with the output current component in steady state. Combining (6) and (7), the capacitor ripple currents can be calculated, after multiplying the capacitor reactance with the ripple currents, the capacitor voltage ripples Δu_{dua} and Δu_{dla} can be deduced as (8) and (9), the summation and difference of upper and lower arm capacitor voltage ripples are calculated as (10) and (11) in the bottom of next page.

$$\begin{bmatrix} i_{sx}(k+1) \\ i_{cx}(k+1) \end{bmatrix} = \begin{bmatrix} 1-\dfrac{RT_s}{\lambda_1 L} & 0 \\ 0 & 1-\dfrac{RT_s}{L} \end{bmatrix}\begin{bmatrix} i_{sx}(k) \\ i_{cx}(k) \end{bmatrix} + \begin{bmatrix} -\dfrac{T_s}{\lambda_1 L} & 0 \\ 0 & -\dfrac{T_s}{2L} \end{bmatrix}\begin{bmatrix} u_{sx}(k) \\ u_{cx}(k) \end{bmatrix} + \begin{bmatrix} \dfrac{2T_s}{\lambda_1 L} & 0 \\ 0 & \dfrac{T_s}{2L} \end{bmatrix}\begin{bmatrix} u_{gx}(k) \\ u_o(k) \end{bmatrix} \tag{5}$$

This article has been accepted for publication in a future issue of this journal, but has not been fully edited. Content may change prior to final publication. Citation information: DOI 10.1109/TPEL.2019.2895224, IEEE Transactions on Power Electronics

III. MODULATED MPC FOR MMC-ACPS

A. Current increments and current tracking errors

Since each arm is consists of N-series SMs, the output voltage level changes from -N to N, the measured SM capacitor voltage of upper and lower arms can be represented by the average voltage of each arm with the voltage balancing control. Then, the output voltage is determined by the output voltage level of upper arm n_{ux} and lower arm n_{lx}, there is

$$\begin{cases} u_{ux} = n_{ux}\, u_{dux}^{ave},\ n_{ux} \in [-N,\cdots,0,\cdots,N] \\ u_{lx} \ = n_{lx}\, u_{dlx}^{ave},\ n_{lx} \in [-N,\cdots,0,\cdots,N] \end{cases} \tag{12}$$

Where u_{dux}^{ave} and u_{dlx}^{ave} are the average capacitor voltage of upper arm and lower arm in the x-phase. Then, the differential mode voltage u_{sx} and common mode voltage u_{cx} are

$$\begin{cases} u_{sx}(k) = u_{dlx}^{ave}(k) n_{lx}(k) - u_{dux}^{ave}(k) n_{ux}(k) \\ u_{cx}(k) = u_{dlx}^{ave}(k) n_{lx}(k) + u_{dux}^{ave}(k) n_{ux}(k) \end{cases} \tag{13}$$

From (13), it can be seen that the number of possible voltage level combinations is $(2N+1)^2$. To reduce the calculation burden, three adjacent voltage level combinations are selected as the finite control set instead of all possible voltage levels in this paper. Voltage level increment Δn_{ux} and Δn_{lx}, namely, the difference between the output voltage level of the current control period and the previous control period, can be derived as

$$\begin{cases} \Delta n_{ux}(k) = n_{ux}(k) - n_{ux}(k\text{-}1),\ \Delta n_{ux} \in [-1,0,1] \\ \Delta n_{lx}\ (k) = n_{lx}(k) - n_{lx}(k\text{-}1),\ \ \Delta n_{lx} \in [-1,0,1] \end{cases} \tag{14}$$

Combining (5), (12)-(14), the currents can be predicted as (15), where $i_{sx}(k+1)|_0$ and $i_{cx}(k+1)|_0$ indicate the predictive currents at the end of (k+1)th control period when the output voltage levels of kth control period equal to the one of previous control period, namely the Δn_{ux} and Δn_{lx} in (14) are equal to 0.

Then, the current tracking errors at the end of (k+1)th instant can be predicted as

$$\begin{cases} e_{rrsx}(k+1) = i_{sx}^{ref}(k+1) - i_{sx}(k+1)|_0 \\ e_{rrcx}(k+1) = i_{cx}^{ref}(k+1) - i_{cx}(k+1)|_0 \end{cases} \tag{16}$$

Combining (14) and (15), the current increments Δi_{slx} and Δi_{clx} caused by the voltage level increment in the lower arm and the ones Δi_{sux} and Δi_{cux} caused by the voltage level increment in the upper arm when Δn_{lx} or Δn_{ux} is equal to 1 or -1 on the basis of $i_{sx}(k+1)|_0$ and $i_{cx}(k+1)|_0$ can be obtained as (17)

$$\begin{cases} i_{sx}(k+1) = i_{sx}(k+1)|_0 - \Delta n_{lx}(k)\Delta i_{slx}(k+1) + \Delta n_{ux}(k)\Delta i_{sux}(k+1) \\ i_{cx}(k+1) = i_{cx}(k+1)|_0 - \Delta n_{lx}(k)\Delta i_{clx}(k+1) - \Delta n_{ux}(k)\Delta i_{cux}(k+1) \end{cases} \tag{17}$$

$$\begin{cases} \Delta i_{slx}(k+1) = \dfrac{T_s}{\lambda_1 L} u_{dlx}^{ave}(k),\ \Delta i_{sux}(k+1) = \dfrac{T_s}{\lambda_1 L} u_{dux}^{ave}(k) \\ \Delta i_{clx}(k+1) = \dfrac{T_s}{\lambda_2 L} u_{dlx}^{ave}(k),\ \Delta i_{cux}(k+1) = \dfrac{T_s}{\lambda_2 L} u_{dux}^{ave}(k) \end{cases} \tag{18}$$

$$\begin{aligned} \Delta u_{dua} = &-\frac{M_c I_s}{8C(\omega_o - \omega_g)}\sin((\omega_o - \omega_g)t + \theta_o - \varphi_{ga}) - \frac{M_s I_o}{12C(\omega_o - \omega_g)}\sin((\omega_o - \omega_g)t + \theta_o + \varphi_o) \\ &+\frac{M_c I_s}{8C(\omega_o + \omega_g)}\sin((\omega_o + \omega_g)t + \theta_o + \varphi_{ga}) + \frac{M_s I_o}{12C(\omega_o + \omega_g)}\sin((\omega_o + \omega_g)t + \theta_o + \varphi_o) \\ &-\frac{M_s I_s}{16C\omega_g}\sin(2\omega_g t + \varphi_{ga}) - \frac{M_c I_o}{24C\omega_o}\sin(2\omega_o t + 2\theta_o + \varphi_o) \end{aligned} \tag{8}$$

$$\begin{aligned} \Delta u_{dla} = &\frac{M_c I_s}{8C(\omega_o - \omega_g)}\sin((\omega_o - \omega_g)t + \theta_o - \varphi_{ga}) + \frac{M_s I_o}{12C(\omega_o - \omega_g)}\sin((\omega_o - \omega_g)t + \theta_o + \varphi_o) \\ &-\frac{M_c I_s}{8C(\omega_o + \omega_g)}\sin((\omega_o + \omega_g)t + \theta_o + \varphi_{ga}) - \frac{M_s I_o}{12C(\omega_o + \omega_g)}\sin((\omega_o + \omega_g)t + \theta_o + \varphi_o) \\ &-\frac{M_s I_s}{16C\omega_g}\sin(2\omega_g t + \varphi_{ga}) - \frac{M_c I_o}{24C\omega_o}\sin(2\omega_o t + 2\theta_o + \varphi_o) \end{aligned} \tag{9}$$

$$\Delta u_{dla} + \Delta u_{dua} = -\frac{M_s I_s}{8C\omega_g}\sin(2\omega_g t + \varphi_{ga}) - \frac{M_c I_o}{12C\omega_o}\sin(2\omega_o t + 2\theta_o + \varphi_o) \tag{10}$$

$$\begin{aligned} \Delta u_{dla} - \Delta u_{dua} = &\frac{M_c I_s}{4C(\omega_o - \omega_g)}\sin((\omega_o - \omega_g)t + \theta_o - \varphi_{ga}) + \frac{M_s I_o}{6C(\omega_o - \omega_g)}\sin((\omega_o - \omega_g)t + \theta_o + \varphi_o) \\ &-\frac{M_c I_s}{4C(\omega_o + \omega_g)}\sin((\omega_o + \omega_g)t + \theta_o + \varphi_{ga}) - \frac{M_s I_o}{6C(\omega_o + \omega_g)}\sin((\omega_o + \omega_g)t + \theta_o + \varphi_o) \end{aligned} \tag{11}$$

$$\begin{cases} i_{sx}(k+1)|_0 = \dfrac{T_s}{\lambda_1 L}[2u_{gx}(k) - u_{dlx}^{ave}(k)n_{lx}(k) + u_{dux}^{ave}(k)n_{ux}(k)] + (1 - \dfrac{RT_s}{\lambda_1 L})i_{sx}(k) \\ i_{cx}(k+1)|_0 = \dfrac{T_s}{2L}[u_o(k) - u_{dlx}^{ave}(k)n_{lx}(k) - u_{dux}^{ave}(k)n_{ux}(k)] + (1 - \dfrac{RT_s}{L})i_{cx}(k) \end{cases} \tag{15}$$

This article has been accepted for publication in a future issue of this journal, but has not been fully edited. Content may change prior to final publication. Citation information: DOI 10.1109/TPEL.2019.2895224, IEEE Transactions on Power Electronics

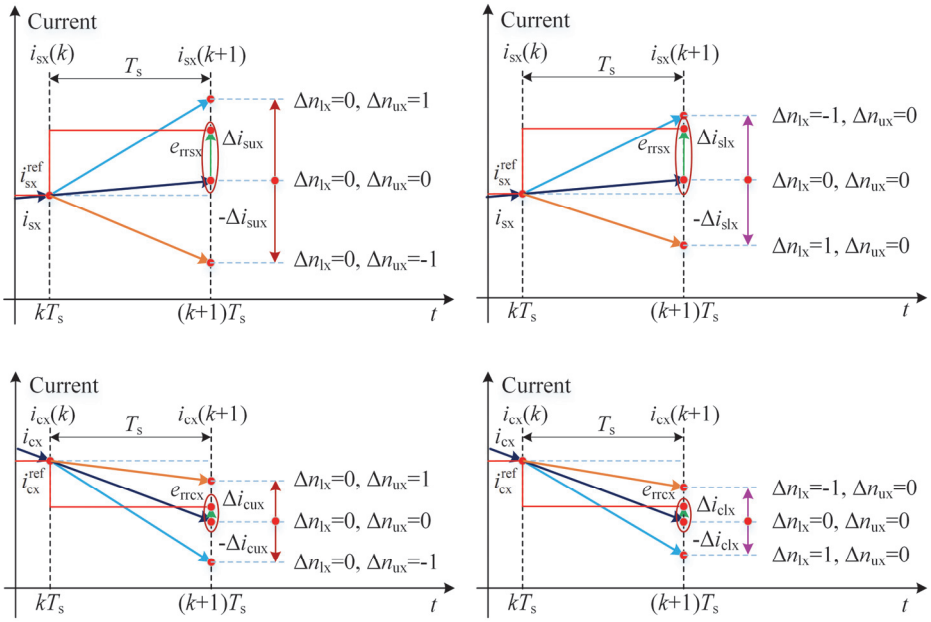

Fig. 2 Current increments and output level increments.

Where $\lambda_2 L=(2L+3L_{load})L/(L+L_{load})$ is the equivalent inductance considering the effect on $u_o(k)$ when $u_{cx}(k)$ stepped. In Fig.2, both i_{slx} and i_{clx} increased when Δn_{lx} =-1, Δn_{ux} =0 and decreased when Δn_{lx}=1, Δn_{ux} =0. But this trend is changed for Δn_{ux}, i_{sux} increased and i_{cux} decreased when Δn_{lx} =0, Δn_{ux} =1, while i_{sux} decreased and i_{cux} increased when Δn_{lx} =0, Δn_{ux} =-1. Combinations of Δn_{ux} and Δn_{lx} with different duty cycles can be employed to eliminate the current tracking errors shown in (16), but there are many possible voltage level increment combinations and the constrains to select the optimal one is unknown.

B. Modulated vectors sequences

In this part, the modulated vectors sequence is built. From (14), the nine combinations of Δn_{lx} and Δn_{ux} are listed in Table I. Each combination can be represented by a vector according to the current increments it caused as shown in Table I. Fig. 3 shows the nine vectors and eight sectors, the $(i_{sx}(k+1)|_0, i_{cx}(k+1)|_0)$ is regarded as the origin of coordinate, and $\boldsymbol{V}_0$ is represented by zero vector. According to the current increments, the plane is divided into eight sectors S_1 to S_8. It is worth mentioning that the boundaries of these sectors are limited by the vectors around the sectors and the line connecting the endpoints of two adjacent vectors.

Based on Fig. 3(a) and (b), the constrains for the eight sectors shown in Table II are built based on the polarity and relationship of the two current errors according to (13) to (18). For example, if both the current errors stratify that $(\Delta i_{clx}-\Delta i_{cux})/(\Delta i_{slx}+\Delta i_{sux})\ e_{rrsx} < e_{rrcx} \leq (\Delta i_{clx}/\Delta i_{slx})\ e_{rrsx}$, therefore (e_{rrsx}, e_{rrcx}) is located in sector 1. If $(\Delta i_{clx}+\Delta i_{cux})/(\Delta i_{slx}-\Delta i_{sux})\ e_{rrsx} < e_{rrcx}$ and $(-\Delta i_{cux}/\Delta i_{sux})\ e_{rrsx} < e_{rrcx}$, then (e_{rrsx}, e_{rrcx}) is located in sector 3. It is worth mentioning that Fig. 3(a) and (b) show the vectors and sectors under the conditions that $(\Delta i_{clx}-\Delta i_{cux})>0$ and $(\Delta i_{slx}-\Delta i_{sux})<0$. When these conditions varied, the location of the endpoints $\boldsymbol{V}_1$, $\boldsymbol{V}_3$, $\boldsymbol{V}_5$ and $\boldsymbol{V}_7$ will change, but the current increments shown in Table I and constrains shown in Table II still hold. Note that

TABLE I
NINE COMBINATIONS AND VECTORS

Δn_{lx}	Δn_{ux}	Vectors	Input current increment	Circulating current increment
-1	1	$\boldsymbol{V}_1$	$\Delta i_{slx}+\Delta i_{sux}$	$\Delta i_{clx}-\Delta i_{cux}$
-1	0	$\boldsymbol{V}_2$	Δi_{slx}	Δi_{clx}
-1	-1	$\boldsymbol{V}_3$	$\Delta i_{slx}-\Delta i_{sux}$	$\Delta i_{clx}+\Delta i_{cux}$
0	-1	$\boldsymbol{V}_4$	$-\Delta i_{sux}$	Δi_{cux}
1	-1	$\boldsymbol{V}_5$	$-\Delta i_{slx}-\Delta i_{sux}$	$-\Delta i_{clx}+\Delta i_{cux}$
1	0	$\boldsymbol{V}_6$	$-\Delta i_{slx}$	$-\Delta i_{clx}$
1	1	$\boldsymbol{V}_7$	$-\Delta i_{slx}+\Delta i_{sux}$	$-\Delta i_{clx}-\Delta i_{cux}$
0	1	$\boldsymbol{V}_8$	Δi_{sux}	$-\Delta i_{cux}$
0	0	$\boldsymbol{V}_0$	0	0

the constrains are the same for sectors S_1, S_4, S_5 and S_8 no matter $\Delta i_{slx}+\Delta i_{sux}$ is equal to or larger or smaller than zero, while the constrains for sectors S_2, S_3, S_6 and S_7 are changed according to $\Delta i_{slx}+\Delta i_{sux}$ as shown in Table II.

According to (18), the summation and the difference of input current increments Δi_{slx} and Δi_{sux} and the ones of circulating current increments Δi_{clx} and Δi_{cux} are related to the summation and the difference of average capacitor voltages of upper and lower arm. When the ripple of capacitor voltage is small compared with the dc voltage, the measured average capacitor voltage of upper and lower arms can be simplified as the average voltage of each phase *u*ave dx. In fact, since the capacitor voltage ripple is included in (15), only one capacitor voltage ripple of upper or lower arm is neglected instead of the voltage ripple of all SMs, because only the three adjacent levels are considered in (14). Under this condition, the current increments in (18) can be simplified as

$$\Delta i_{sx}(k+1)=\frac{T_s}{\lambda_1 L}u_{dx}^{ave}(k),\ \Delta i_{cx}(k+1)=\frac{T_s}{\lambda_2 L}u_{dx}^{ave}(k) \tag{19}$$

This article has been accepted for publication in a future issue of this journal, but has not been fully edited. Content may change prior to final publication. Citation information: DOI 10.1109/TPEL.2019.2895224, IEEE Transactions on Power Electronics

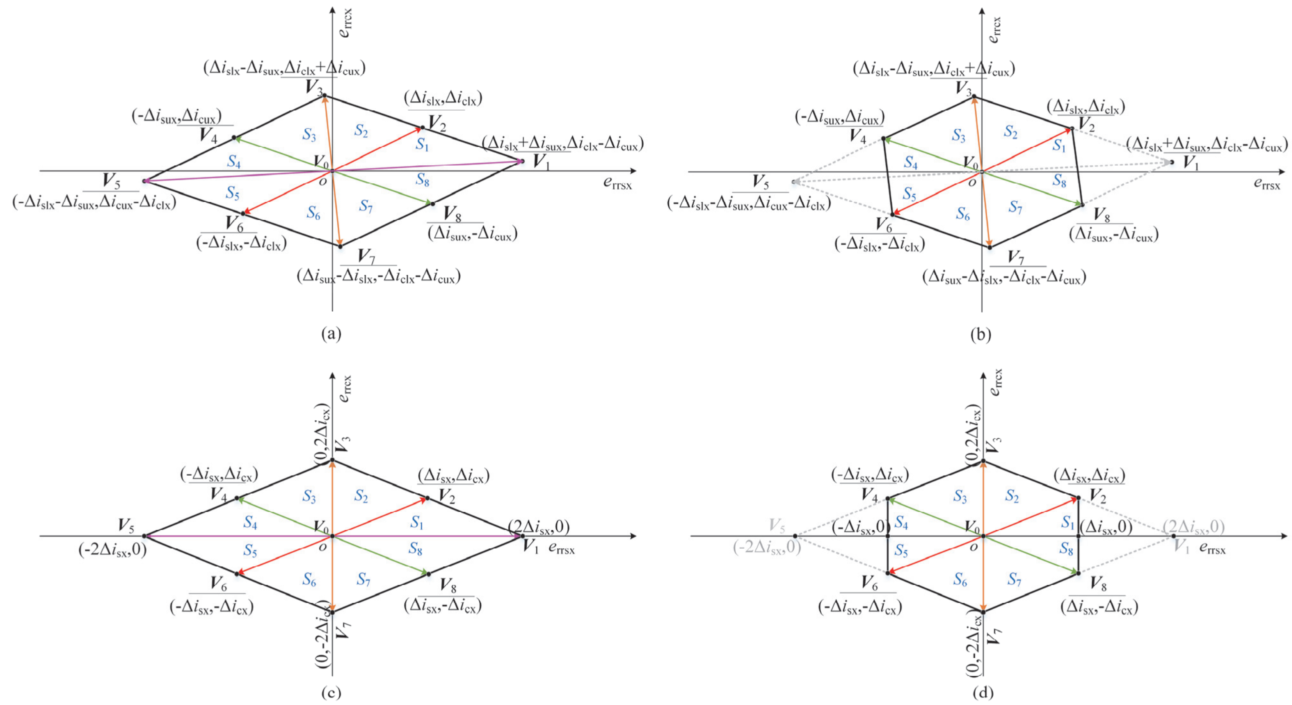

Fig. 3 Vectors and sectors. (a) MMPC approach I considering the SM voltage ripple. (b) MMPC approach II considering the SM voltage ripple. (c) MMPC approach I simplifying the SM voltage ripple. (d) MMPC approach II simplifying the SM voltage ripple.

TABLE II
CONSTRAINS FOR EIGHT SECTORS

Sectors	Relation of e_{rrcx} and e_{rrsx} (when Δi_{slx}-Δi_{sux}>0)	Relation of e_{rrcx} and e_{rrsx} (when Δi_{slx}-Δi_{sux}<0)	Relation of e_{rrcx} and e_{rrsx} (when Δi_{slx}-Δi_{sux}=0)
S_1	$\frac{\Delta i_{clx}-\Delta i_{cux}}{\Delta i_{slx}+\Delta i_{sux}}e_{rrsx}<e_{rrcx}\le\frac{\Delta i_{clx}}{\Delta i_{slx}}e_{rrsx}$	$\frac{\Delta i_{clx}-\Delta i_{cux}}{\Delta i_{slx}+\Delta i_{sux}}e_{rrsx}<e_{rrcx}\le\frac{\Delta i_{clx}}{\Delta i_{slx}}e_{rrsx}$	$\frac{\Delta i_{clx}-\Delta i_{cux}}{\Delta i_{slx}+\Delta i_{sux}}e_{rrsx}<e_{rrcx}\le\frac{\Delta i_{clx}}{\Delta i_{slx}}e_{rrsx}$
S_2	$\frac{\Delta i_{clx}}{\Delta i_{slx}}e_{rrsx}<e_{rrcx}\le\frac{\Delta i_{clx}+\Delta i_{cux}}{\Delta i_{slx}-\Delta i_{sux}}e_{rrsx}$	$\frac{\Delta i_{clx}+\Delta i_{cux}}{\Delta i_{slx}-\Delta i_{sux}}e_{rrsx}\le e_{rrcx}$ and $\frac{\Delta i_{clx}}{\Delta i_{slx}}e_{rrsx}<e_{rrcx}$	$e_{rrsx}\ge0$, $e_{rrcx}\ge0$ and $\frac{\Delta i_{clx}}{\Delta i_{slx}}e_{rrsx}<e_{rrcx}$
S_3	$\frac{\Delta i_{clx}+\Delta i_{cux}}{\Delta i_{slx}-\Delta i_{sux}}e_{rrsx}<e_{rrcx}$ and $-\frac{\Delta i_{cux}}{\Delta i_{sux}}e_{rrsx}\le e_{rrcx}$	$-\frac{\Delta i_{clx}}{\Delta i_{slx}}e_{rrsx}\le e_{rrcx}<\frac{\Delta i_{clx}+\Delta i_{cux}}{\Delta i_{slx}-\Delta i_{sux}}e_{rrsx}$	$e_{rrsx}<0$, $e_{rrcx}\ge0$ and $-\frac{\Delta i_{clx}}{\Delta i_{slx}}e_{rrsx}<e_{rrcx}$
S_4	$\frac{-\Delta i_{clx}+\Delta i_{cux}}{-\Delta i_{slx}-\Delta i_{sux}}e_{rrsx}\le e_{rrcx}<-\frac{\Delta i_{cux}}{\Delta i_{sux}}e_{rrsx}$	$\frac{-\Delta i_{clx}+\Delta i_{cux}}{-\Delta i_{slx}-\Delta i_{sux}}e_{rrsx}\le e_{rrcx}<-\frac{\Delta i_{cux}}{\Delta i_{sux}}e_{rrsx}$	$\frac{-\Delta i_{clx}+\Delta i_{cux}}{-\Delta i_{slx}-\Delta i_{sux}}e_{rrsx}\le e_{rrcx}<-\frac{\Delta i_{cux}}{\Delta i_{sux}}e_{rrsx}$
S_5	$\frac{-\Delta i_{clx}}{-\Delta i_{slx}}e_{rrsx}\le e_{rrcx}<\frac{-\Delta i_{clx}+\Delta i_{cux}}{-\Delta i_{slx}-\Delta i_{sux}}e_{rrsx}$	$\frac{-\Delta i_{clx}}{-\Delta i_{slx}}e_{rrsx}\le e_{rrcx}<\frac{-\Delta i_{clx}+\Delta i_{cux}}{-\Delta i_{slx}-\Delta i_{sux}}e_{rrsx}$	$\frac{-\Delta i_{clx}}{-\Delta i_{slx}}e_{rrsx}\le e_{rrcx}<\frac{-\Delta i_{clx}+\Delta i_{cux}}{-\Delta i_{slx}-\Delta i_{sux}}e_{rrsx}$
S_6	$\frac{-\Delta i_{clx}-\Delta i_{cux}}{-\Delta i_{slx}+\Delta i_{sux}}e_{rrsx}\le e_{rrcx}<\frac{-\Delta i_{cux}}{-\Delta i_{sux}}e_{rrsx}$	$e_{rrcx}<\frac{-\Delta i_{clx}}{-\Delta i_{slx}}e_{rrsx}$ and $e_{rrcx}\le\frac{-\Delta i_{clx}-\Delta i_{cux}}{-\Delta i_{slx}+\Delta i_{sux}}e_{rrsx}$	$e_{rrsx}<0$, $e_{rrcx}<0$ and $e_{rrcx}<\frac{\Delta i_{clx}}{\Delta i_{slx}}e_{rrsx}$
S_7	$e_{rrcx}<\frac{-\Delta i_{clx}-\Delta i_{cux}}{-\Delta i_{slx}+\Delta i_{sux}}e_{rrsx}$ and $e_{rrcx}\le-\frac{\Delta i_{cux}}{\Delta i_{sux}}e_{rrsx}$	$\frac{-\Delta i_{clx}-\Delta i_{cux}}{-\Delta i_{slx}+\Delta i_{sux}}e_{rrsx}<e_{rrcx}\le-\frac{\Delta i_{clx}}{\Delta i_{slx}}e_{rrsx}$	$e_{rrsx}\ge0$, $e_{rrcx}<0$ and $e_{rrcx}\le-\frac{\Delta i_{clx}}{\Delta i_{slx}}e_{rrsx}$
S_8	$-\frac{\Delta i_{cux}}{\Delta i_{sux}}e_{rrsx}<e_{rrcx}\le\frac{\Delta i_{clx}-\Delta i_{cux}}{\Delta i_{slx}+\Delta i_{sux}}e_{rrsx}$	$-\frac{\Delta i_{cux}}{\Delta i_{sux}}e_{rrsx}<e_{rrcx}\le\frac{\Delta i_{clx}-\Delta i_{cux}}{\Delta i_{slx}+\Delta i_{sux}}e_{rrsx}$	$-\frac{\Delta i_{cux}}{\Delta i_{sux}}e_{rrsx}<e_{rrcx}\le\frac{\Delta i_{clx}-\Delta i_{cux}}{\Delta i_{slx}+\Delta i_{sux}}e_{rrsx}$

This article has been accepted for publication in a future issue of this journal, but has not been fully edited. Content may change prior to final publication. Citation information: DOI 10.1109/TPEL.2019.2895224, IEEE Transactions on Power Electronics

With (19), the nine vectors and eight sectors shown in Fig. 3(a) and (b) can be simplified as Fig. 3(c) and (d). Note that this simplified approach can be regard as a special solution of the proposed MMPC, this paper mainly focuses on the general way.

To eliminate the two current tracking errors at the end of each control period simultaneously, a modulated vector sequence consisting of zero vector and two active vectors $\boldsymbol{V}_M$ and $\boldsymbol{V}_L$ with different duty cycles can be employed according to Fig. 3. The two active vectors are selected by determining which sector the errors (e_{rrsx}, e_{rrcx}) belong to, then the two vectors around this sector are picked as the active vectors $\boldsymbol{V}_M$ and $\boldsymbol{V}_L$ as shown in Table III. For example, if (e_{rrsx}, e_{rrcx}) is located in sector 1 in Fig. 3(a), therefore $\boldsymbol{V}_0$, $\boldsymbol{V}_2$ and $\boldsymbol{V}_1$ are selected as the zero vector and two active vectors $\boldsymbol{V}_M$ and $\boldsymbol{V}_L$.

While, the norms of $\boldsymbol{V}_1$ and $\boldsymbol{V}_5$ are quite longer than others as shown in Fig. 3(a) and (c) when the grid side inductance is small and $2L_g$ is quite less than L. If these vectors are selected, current tracking errors can be removed at the end of each control period, but large current ripples will be caused by the long norm vectors during their applied duty cycles. To deal with this condition, a new MMPC approach is also proposed, seven vectors except $\boldsymbol{V}_1$ and $\boldsymbol{V}_5$ are utilized as shown in Fig.3(b) and (d), and the boundary conditions become: ($-\Delta i_{cux}/\Delta i_{sux}$) e_{rrsx} < $e_{rrcx} \le (\Delta i_{clx}/\Delta i_{slx})$ e_{rrsx} for S_1 and S_8, ($\Delta i_{clx}/\Delta i_{slx}$) e_{rrsx} < $e_{rrcx} \le$ ($-\Delta i_{cux}/\Delta i_{sux}$) for S_4 and S_5. The other differences of two proposed methods are the selection of active vectors for S_1, S_4, S_5 and S_8 as shown in Table III.

C. Duty cycle calculation

In this part, the proposed MMPC calculates the duty cycles for the vectors during one control period in order to regulate the input current and circulating current to the desired reference values simultaneously at the end of each control period. If (e_{rrsx}, e_{rrcx}) is located in the eight sectors, combination of zero vector and two active vectors are employed as shown in Fig. 4(a). Three duty cycles, d_1 for zero vector, d_2 for the active vector $\boldsymbol{V}_M$ and d_3 for the active vector $\boldsymbol{V}_L$, are calculated. The applying sequences of the three vectors are also shown in Table III for each sector. Taking S_1 for example, $\boldsymbol{V}_0$ is applied during the start to d_1T_s interval in the kth control period, and $\boldsymbol{V}_2$ is applied during the d_1T_s to the (d_1T_s+d_2T_s) interval in the control period, then $\boldsymbol{V}_1$ for approach I and $\boldsymbol{V}_8$ for approach II are applied from the (d_1T_s+d_2T_s) instant to the end of the (k+1)th control period as shown in Fig. 4(b).

A modulated vector sequence consisting of zero vector and two active vectors $\boldsymbol{V}_M$ and $\boldsymbol{V}_L$ with different duty cycles is employed to eliminate the input and circulating current errors. The vector sequences for the eight sectors are illustrated in Table III and the input current and circulating increments caused by each vector are shown in Table I. Assuming that Δi_{sxM} and Δi_{cxM} are the current increments caused by active vector $\boldsymbol{V}_M$, and Δi_{sxL} and Δi_{cxL} are the ones caused by active vector $\boldsymbol{V}_L$. Then, the general current increments equation can be expressed as

$$\begin{cases} d_2\Delta i_{sxM}(k+1)+d_3\Delta i_{sxL}(k+1)=e_{rrsx}(k+1) \\ d_2\Delta i_{cxM}(k+1)+d_3\Delta i_{cxL}(k+1)=e_{rrcx}(k+1) \end{cases} \quad (20)$$

TABLE III
MODULATED VECTOR SEQUENCES

MMPC approach I		MMPC approach II	
Sector	Vectors $\boldsymbol{V}_0$, $\boldsymbol{V}_M$, $\boldsymbol{V}_L$	Sector	Vectors $\boldsymbol{V}_0$, $\boldsymbol{V}_M$, $\boldsymbol{V}_L$
S_1	$\boldsymbol{V}_0$, $\boldsymbol{V}_2$, $\boldsymbol{V}_1$	S_1	$\boldsymbol{V}_0$, $\boldsymbol{V}_2$, $\boldsymbol{V}_8$
S_2	$\boldsymbol{V}_0$, $\boldsymbol{V}_2$, $\boldsymbol{V}_3$	S_2	$\boldsymbol{V}_0$, $\boldsymbol{V}_2$, $\boldsymbol{V}_3$
S_3	$\boldsymbol{V}_0$, $\boldsymbol{V}_4$, $\boldsymbol{V}_3$	S_3	$\boldsymbol{V}_0$, $\boldsymbol{V}_4$, $\boldsymbol{V}_3$
S_4	$\boldsymbol{V}_0$, $\boldsymbol{V}_4$, $\boldsymbol{V}_5$	S_4	$\boldsymbol{V}_0$, $\boldsymbol{V}_4$, $\boldsymbol{V}_6$
S_5	$\boldsymbol{V}_0$, $\boldsymbol{V}_6$, $\boldsymbol{V}_5$	S_5	$\boldsymbol{V}_0$, $\boldsymbol{V}_4$, $\boldsymbol{V}_6$
S_6	$\boldsymbol{V}_0$, $\boldsymbol{V}_6$, $\boldsymbol{V}_7$	S_6	$\boldsymbol{V}_0$, $\boldsymbol{V}_6$, $\boldsymbol{V}_7$
S_7	$\boldsymbol{V}_0$, $\boldsymbol{V}_8$, $\boldsymbol{V}_7$	S_7	$\boldsymbol{V}_0$, $\boldsymbol{V}_8$, $\boldsymbol{V}_7$
S_8	$\boldsymbol{V}_0$, $\boldsymbol{V}_8$, $\boldsymbol{V}_1$	S_8	$\boldsymbol{V}_0$, $\boldsymbol{V}_2$, $\boldsymbol{V}_8$

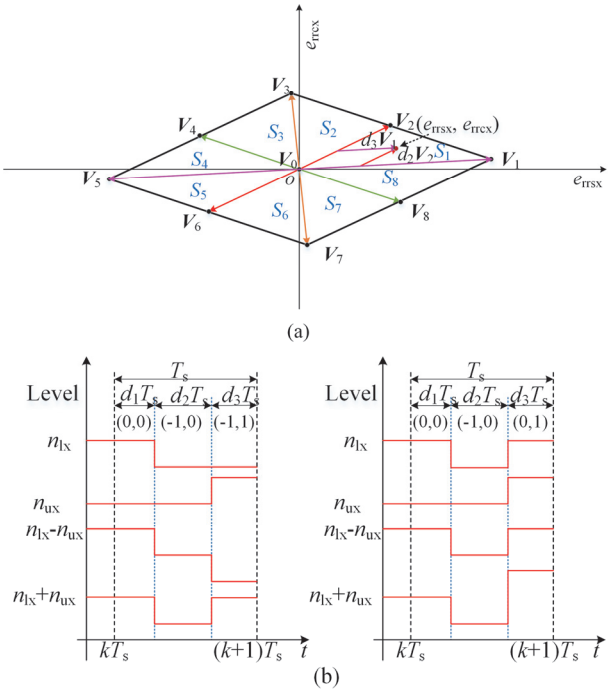

Fig. 4 Current tracking errors eliminating. (a) Combination of zero vector and two active vectors in a sector. (b) Applying sequences of the three vectors.

Combining (20) with the vector sequences and eight sectors shown in Table III and the current increments shown in Table I, the general duty cycles equations can be calculated as

$$d_2=\frac{e_{rrsx}(k+1)\Delta i_{cxL}(k+1)-e_{rrcx}(k+1)\Delta i_{sxL}(k+1)}{\Delta i_{sxM}(k+1)\Delta i_{cxL}(k+1)-\Delta i_{cxM}(k+1)\Delta i_{sxL}(k+1)} \quad (21)$$

$$d_3=\frac{e_{rrsx}(k+1)\Delta i_{cxM}(k+1)-e_{rrcx}(k+1)\Delta i_{sxM}(k+1)}{\Delta i_{sxL}(k+1)\Delta i_{cxM}(k+1)-\Delta i_{cxL}(k+1)\Delta i_{sxM}(k+1)} \quad (22)$$

It is worth mentioning that it is hard to eliminate the current errors if (e_{rrsx}, e_{rrcx}) is not located inside the eight sectors, the summation of d_2 and d_3 obtained by (21) and (22) will be larger than 1, then, d_1 is set to zero, and the others are reduced as

$$d_2=d_2/(d_2+d_3),\ d_3=d_3/(d_2+d_3) \quad (23)$$

Fig. 5(b) and (c) shows the operation principle of proposed methods. The operation process includes three steps as follows

This article has been accepted for publication in a future issue of this journal, but has not been fully edited. Content may change prior to final publication. Citation information: DOI 10.1109/TPEL.2019.2895224, IEEE Transactions on Power Electronics

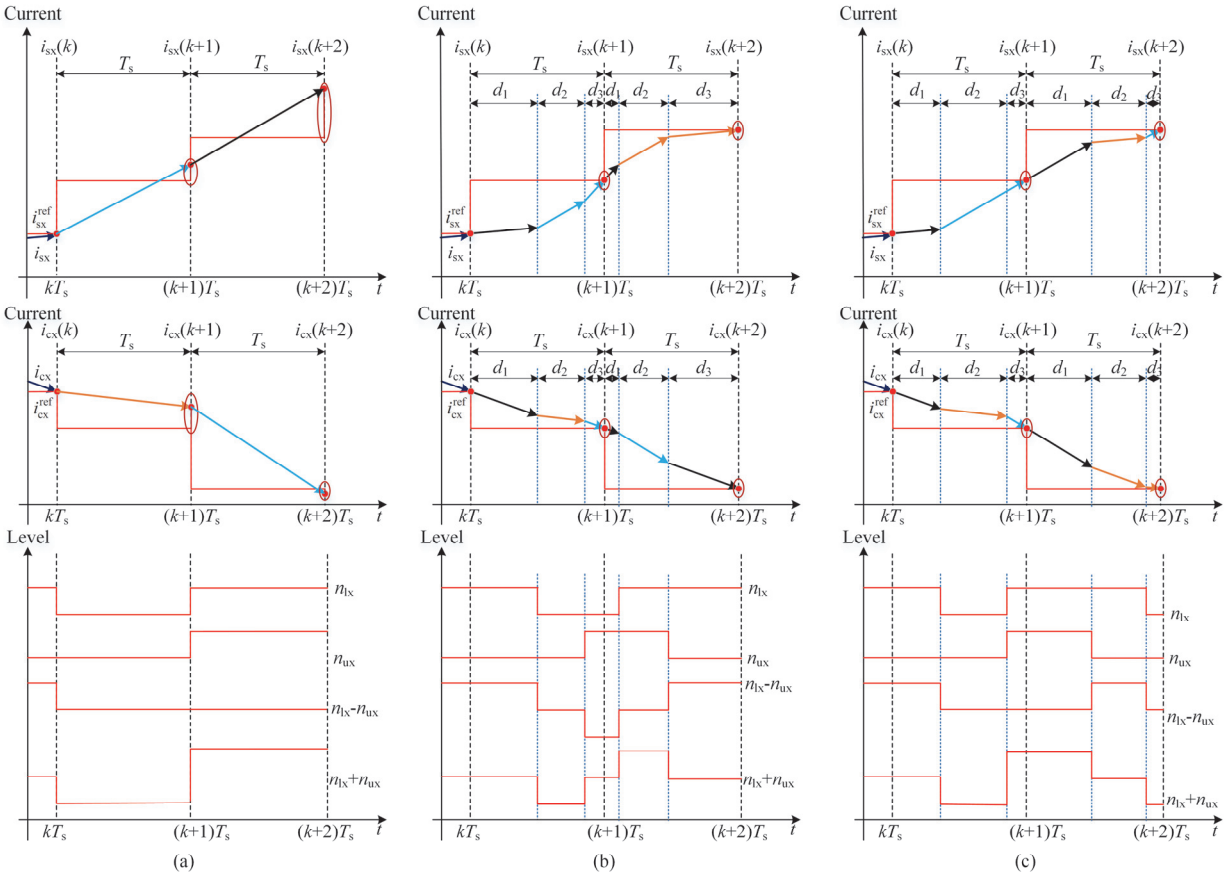

Fig. 5 Operation principle of the conventional and proposed methods (a) Conventional FCS-MPC. (b) Proposed MMPC approach I. (c) Proposed MMPC approach II.

(a) At the end of kth control period, the two current errors are predicted. As shown in Fig. 5, both e_{rrsx} and e_{rrcx} fulfilled that $(\Delta i_{\mathrm{clx}}-\Delta i_{\mathrm{cux}})/(\Delta i_{\mathrm{slx}}+\Delta i_{\mathrm{sux}})\ e_{\mathrm{rrsx}} < e_{\mathrm{rrcx}} \leq (\Delta i_{\mathrm{clx}}/\Delta i_{\mathrm{slx}})\ e_{\mathrm{rrsx}}$, then ($e_{\mathrm{rrsx}}$, e_{rrcx}) is located in S_1.

(b) According to Table I to III, V_2 and V_1 are selected as the active vectors $\boldsymbol{V}_{\mathrm{M}}$ and $\boldsymbol{V}_{\mathrm{L}}$ in MMPC approach I, V_2 and V_8 are selected as the active vectors $\boldsymbol{V}_{\mathrm{M}}$ and $\boldsymbol{V}_{\mathrm{L}}$ in MMPC approach II.

(c) Then, three duty cycles for the zero vector and the two active vectors are calculated according to (21) and (22). Therefore, three level increment combinations (0, 0), (-1, 0) and (-1, 1) with different duty cycles are applied to the converter at the (k+1)th control period in MMPC approach I, (0, 0), (-1, 0) and (0, 1) are applied in MMPC approach II.

Although, vectors with duty cycles are also used to improve current control performance in [37] and [38], the proposed MMPC for MMC-ACPS incorporates several innovative ideas. In [37], the vector applied at the end of the previous control period along with its two adjacent vectors are combined to eliminate the current tracking error for a single phase cascaded H-Bridge converter. The main similarities and differences of the methods in [37] and this paper are: 1) three adjacent voltage levels are utilized in both methods, there is three vectors in accordance with the levels in [37] while the number of possible vectors increases to nine in this paper. 2) the selection of optimal vectors combination becomes quite complex because both the input current and circulating current can be regulated by each vector. 3) input current tracking error is eliminated at the end of each control period in [37] while both the input current and circulating current tracking errors are eliminated simultaneously with the proposed methods. In [38], a MMPC is proposed for MMC in HVDC application, but the input current control and circulating current control are independent and the circulating current is regulated by only one extra SM which is quite different with the methods proposed in this paper.

The operation principle of conventional method is shown in Fig. 5(a). In conventional FCS-MPC, cost function to optimize the input current and circulating current is evaluated for the nine voltage level increment combinations, the one which minimize the cost function is selected as the optimal combination and applied in the next control period. The cost function designed in the conventional method is shown as follows

$$g = c_1\left|i_{\mathrm{sx}}^{\mathrm{ref}}(k+1)-i_{\mathrm{sx}}(k+1)\right|+c_2\left|i_{\mathrm{cx}}^{\mathrm{ref}}(k+1)-i_{\mathrm{cx}}(k+1)\right| \quad (24)$$

Where c_1 and c_2 are weighting factors of input current and circulating current. As shown in Fig. 5(a), voltage level increment combination (-1, 0) is chose as the optimal one in (k)th control period, therefore, the output voltage level of lower arm reduces one while the upper arm remains unchanged. In (k+1)th control period, (1, 1) is selected, then, both the output voltage level of upper and lower arm increase one.

This article has been accepted for publication in a future issue of this journal, but has not been fully edited. Content may change prior to final publication. Citation information: DOI 10.1109/TPEL.2019.2895224, IEEE Transactions on Power Electronics

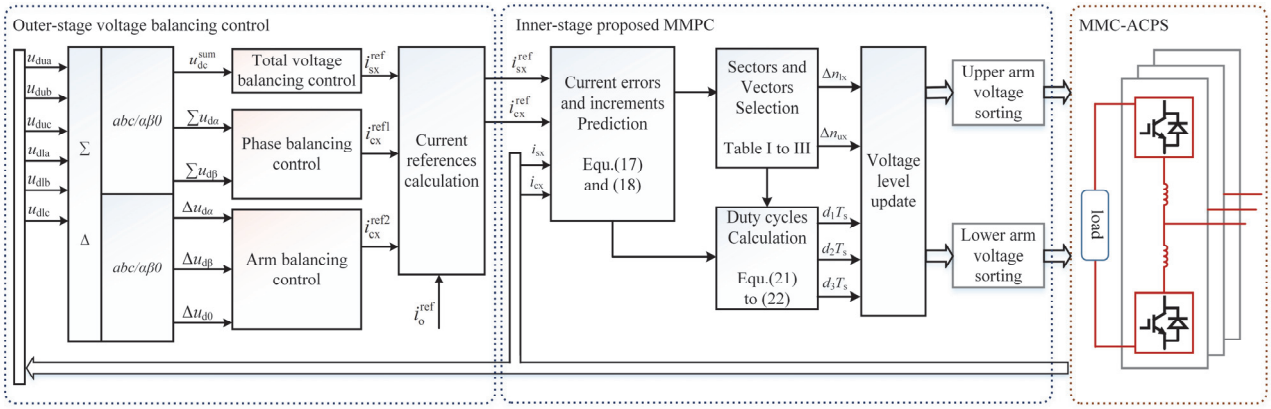

Fig. 6 Control strategy diagram of MMC-ACPS with proposed MMPC.

From Fig. 5(a), it can be known that there is one switch action at most in the upper and lower arm respectively for each control period. Therefore, the average switching frequency (ASF)[29] is less than the half of control frequency in conventional method. While, one switch action is executed in the upper and lower arm respectively for each control period in MMPC approach I, therefore, the ASF of MMPC approach I is equal the half of the control frequency. In MMPC approach II, two switch actions are applied in the upper arm for (k+1)th control period while one switch action is executed in the lower arm. As a consequence, MMPC approach II presents higher ASF than approach I. Note that approach II has the same vector sequence as approach I in sectors S_2, S_3, S_6 and S_7. Then, the ASF of MMPC approach II is less than 150% of the approach I.

It is worth mentioning that the control delay is not considered in Fig. 5. The one-step delay compensation algorithm presented in [33] is utilized in this paper to compensate the control delay.

IV. Control Strategy of MMC-ACPS

In this paper, a cascaded two-stage control strategy is investigated, capacitor voltage balancing is in the outer-stage, input currents and circulating current are regulated by the proposed methods in the inner-stage as shown in Fig.6. Input current references are calculated by the total voltage balancing control, circulating current references are obtained according to the output current references along with arm balancing control and phase voltage balancing control. In the inner-stage, input current and circulating current are tracked simultaneously by the proposed methods to determines the optimal number of output voltage level for each arm, then the output voltage level is distributed by sorting algorithm to keep SM capacitor voltages balance.

More specifically, the capacitor voltage balancing control consists of three parts: total voltage balancing control, arm balancing control and phase balancing control. Total voltage control is utilized to keep the summation of all SM capacitor voltages steady and transmit the energy from grid to the load. Arm balancing control is utilized to eliminate the average voltage deviations between the upper and lower arm. The circulating current components i_{cx}^{1} which have the same frequency as grid voltage are employed in the arm balancing control. Phase balancing control is utilized to eliminate the average voltage deviations of the three phases. The circulating current components i_{cx}^{2} which have the same frequency as output current are employed in this balancing control.

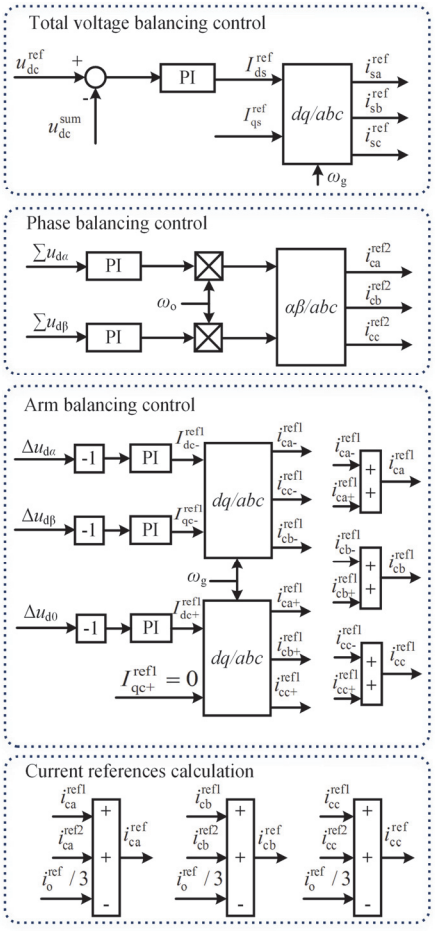

Fig. 7 Voltage balancing control diagram of MMC-ACPS.

In total voltage control, the error between the reference u_{dc}^{ref} and the average summation voltage u_{dc}^{sum} of three phases is regarded as the input of the PI controller, then the output is

This article has been accepted for publication in a future issue of this journal, but has not been fully edited. Content may change prior to final publication. Citation information: DOI 10.1109/TPEL.2019.2895224, IEEE Transactions on Power Electronics

treated as the active power current references I_{ds}^{ref} of *d*-axis as shown in Fig. 7. To achieve the unit power factor, I_{qs}^{ref} is set as zero. After the *dq*/*abc* transformation, the current references of input current are obtained. It can be seen that the total voltage control regulates the input power of three phase.

In the arm balancing control, voltage difference Δu_{dx} between the upper and lower arm is calculated and transformed to $\Delta u_{d\alpha}$, $\Delta u_{d\beta}$ and Δu_{d0} in the αβ0 frame. To eliminate those voltage deviations, PI controllers are also utilized as shown in Fig. 7. Note that, the internal circulating current components i_{cx}^{1} are divided into symmetrical components (positive and negative sequence components), the negative sequence components are used to dispel $\Delta u_{d\alpha}$ and $\Delta u_{d\beta}$, while the positive sequence component is used to control the common-mode power Δu_{d0} deviation. After the negative and positive sequence *dq*/*abc* transformation, the references of circulating current components i_{cx}^{ref1} are obtained.

In the phase balancing control, voltage summations $\sum u_{dx}$ of the upper and lower arm in the three phases are calculated and transformed to $\Delta u_{d\alpha}$ and $\Delta u_{d\beta}$ in the αβ frame. To suppress those voltage deviations, PI controllers are used and the outputs are multiplied with the synchronous signal of output voltage. After the *αβ*/*abc* transformation, the references of circulating current components i_{cx}^{ref2} are obtained. It is worth mentioning that the voltage balancing control has been discussed and further derivations can be found in [7]. Note that the filtered DC offsets of capacitor voltage signals are used to achieve the branch energy balancing, because the capacitor voltage ripples will introduce harmonic current components to the current references if the ripples are included in the voltage control loop.

V. Experiment Results

To verify the performance of the proposed control method, a 15kW down-scaled physical prototype is developed in the laboratory as shown in Fig. 8. It mainly includes three phases and the digital control system consists of FPGA and DSP. Multimode optical fibers are used to transmit submodule voltage signals, control signals and other signals between main power circuit and control circuit. Parameters are shown in Table IV. Load frequency is set as 120Hz according to requirement of induction heating molten steel. The weighting factors are designed as c_1=6 and c_2=1 considering the input current and output current control performance synthetically in conventional MPC. Digital low-pass filters are used to filter the capacitor voltage ripples. A first-order low-pass filter is added to the arm voltages feedback loop, the cut-off frequency of low-pass filter is design as 50Hz for total voltage balancing control, the cut-off frequency of low-pass filter is design as 15Hz for phase balancing and 6Hz for arm balancing control.

The proposed MMPC along with the conventional FCS-MPC are tested, capacitor voltage ripples are considered in the experiment. Steady-state input currents and single-phase output current of MMC-ACPS are presented in Fig. 9 and Fig. 10. As shown in Fig. 9, currents of MMPC approach I and approach II show smaller current ripples comparing to the

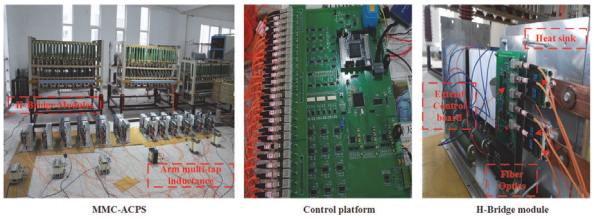

Fig. 8 Experimental setup of MMC-ACPS.

TABLE IV
PARAMETERS OF PROTOTYPE

Parameters	Value
Grid line voltage	380V
Grid frequency(*f*)	50Hz
Sub-module capacitance(*C*)	1100uF
Unit capacitance constant [41]	45ms
Bridge arm inductance(*L*)	3mH
Module Number of cluster (*N*)	2
Load inductance and resistance	1mH and 8Ω
Rated frequency for load current (f_o)	120Hz
Current magnitude for load (I_o)	60A
Module capacitor voltage reference	320V
Current control frequency (f_c)	10kHz

TABLE V
THD AND ASF COMPARISON OF THREE MPC METHODS

	Input currents THD	Output current THD	ASF
Conventional MPC	8.4%, 8.5%, 8.4%	7.3%	2.81kHz
MMPC approach I	6.0%, 5.7%, 5.8%	2.8%	4.82kHz
MMPC approach II	3.5%, 3.3%, 3.4%	3.7%	5.39kHz

currents of conventional method, indicating that current tracking errors are reduced under the control of the proposed methods. While, the input currents of approach I in Fig. 9(b) have more high-frequency components than the ones of approach II in Fig. 9(c), this is because the larger current increments caused by these vectors with long norms are utilized in approach I.

With the same control frequency, conventional MPC method yields many low order harmonics because only one vector determined by the cost function is applied during the entire sampling period, while low order harmonics are eliminated by the modulated vectors sequence with duty cycles in the proposed methods. THD values and ASF of these currents are listed in Table V, the MMPC approach II shows better input current control performance and highest ASF, while MMPC approach I has lower THD value of output current. The multilevel waves of u_{sa} and u_{ca} are shown in Fig. 11 respectively, the waves show higher switching frequency with the proposed methods. Fig.12 shows the capacitor voltage of one SM in the upper and lower arm with these control methods, capacitor voltages are balanced in the experiments.

This article has been accepted for publication in a future issue of this journal, but has not been fully edited. Content may change prior to final publication. Citation information: DOI 10.1109/TPEL.2019.2895224, IEEE Transactions on Power Electronics

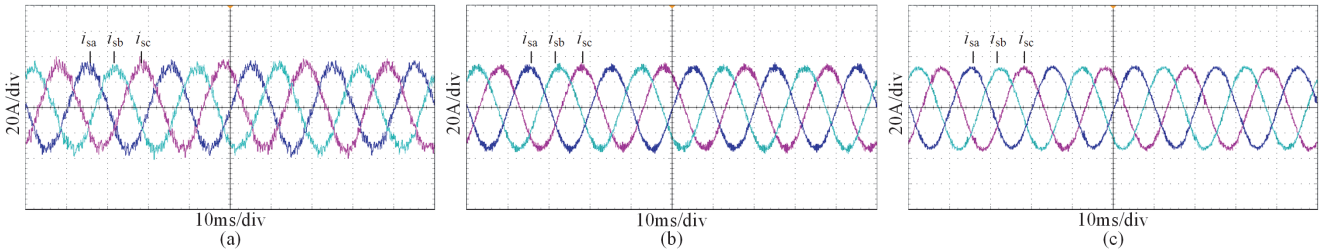

Fig. 9 Experimental waveforms of input currents. (a) Conventional MPC. (b) Proposed MMPC approach I. (c) Proposed MMPC approach II.

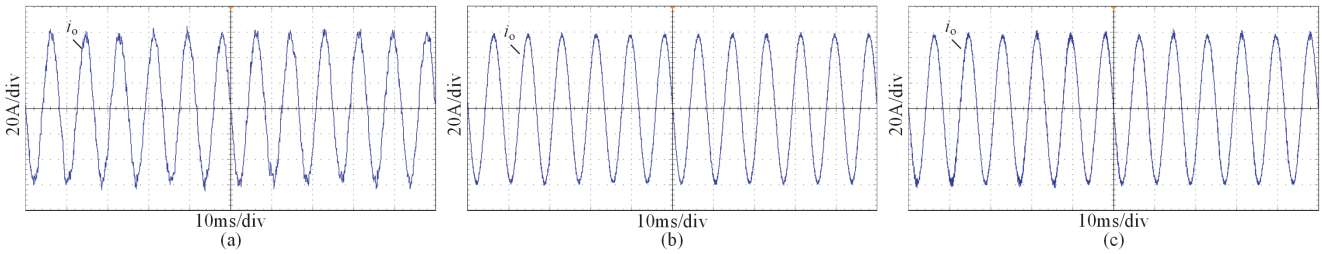

Fig. 10 Experimental waveforms of output current. (a) Conventional MPC. (b) Proposed MMPC approach I. (c) Proposed MMPC approach II.

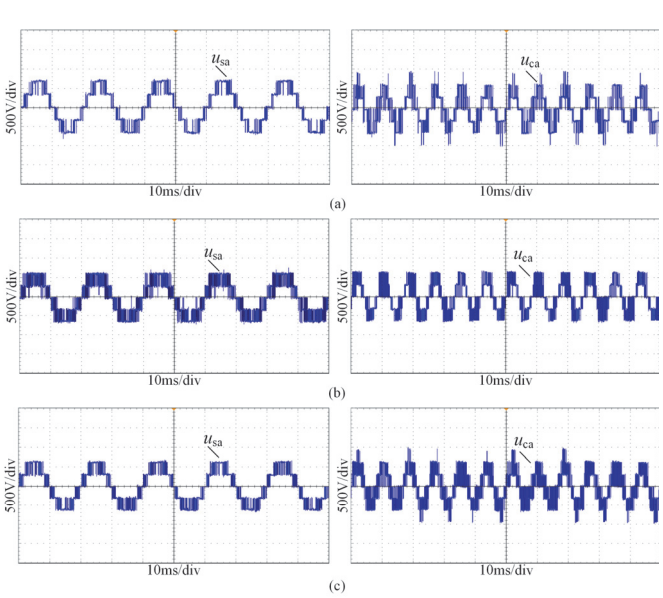

Fig. 11 Experimental multilevel waveforms. (a) Conventional MPC. (b) Proposed MMPC approach I. (c) Proposed MMPC approach II.

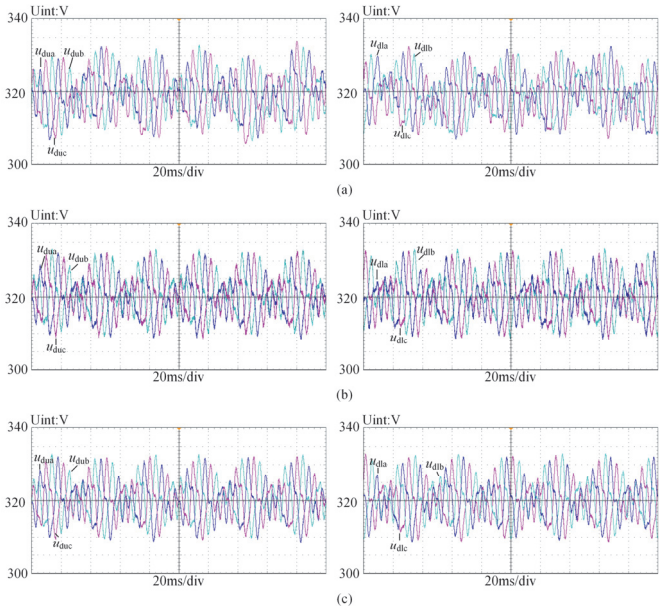

Fig. 12 Experimental waveforms of capacitor voltage. (a) Conventional MPC. (b) Proposed MMPC approach I. (c) Proposed MMPC approach II.

Current THD values and ASF curves of the three methods under various control frequencies are shown in Fig. 13(a) to (c). It can be seen that the proposed two MMPC methods introduce more switching actions to eliminate the current tracking errors and present better current control performance and higher ASF than the conventional method at the same control frequency, thereby these methods reduce the requirement of control frequency of MPC. According to Fig. 13, current THD values with similar ASF of the three methods are listed in Table VI, since three vectors with various duty cycles instead of one vector are employed in the proposed method, the MMPC approach I and approach II shows better current control performance than conventional method when these methods have similar ASF as shown in Table VI.

TABLE VI
THD COMPARISON WITH SIMILAR ASF OF THREE MPC METHODS

	ASF	THD of i_{sc}	THD of i_o	Control Frequency f_c
Conventional MPC	3.25kHz	8.0%	6.8%	11kHz
MMPC approach I	3.01kHz	7.8%	4.2%	6kHz
Conventional MPC	3.42kHz	7.4%	6.5%	12kHz
MMPC approach II	3.28kHz	5.1%	6.2%	6kHz

Apart from the steady-state performance comparison, the dynamic responses to stepped change in output current amplitude from 60A to -60A are also presented. As shown in Fig. 14, the output current controlled by the conventional method presents the best dynamic performance because its level increment duty cycle is not limited. While, the proposed MMPC approach

This article has been accepted for publication in a future issue of this journal, but has not been fully edited. Content may change prior to final publication. Citation information: DOI 10.1109/TPEL.2019.2895224, IEEE Transactions on Power Electronics

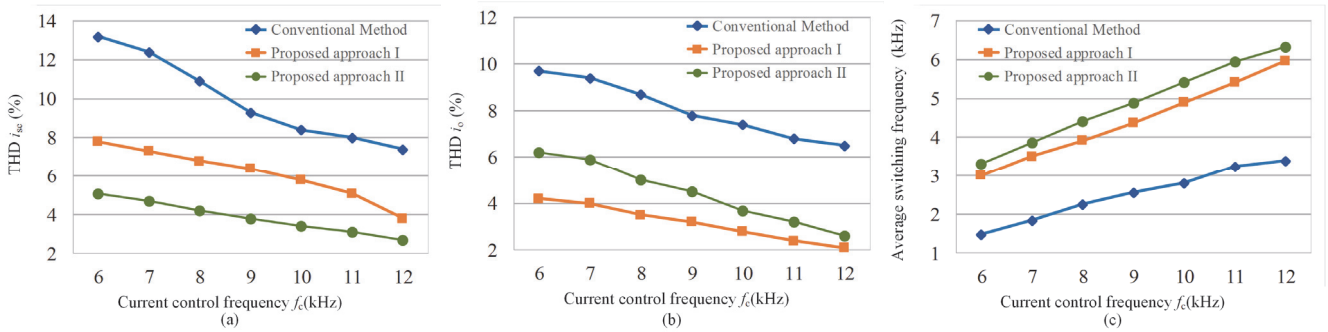

Fig. 13 Curves of the THD values and average switching frequency. (a) Input current THD. (b) Output current THD. (c) Average switching frequency.

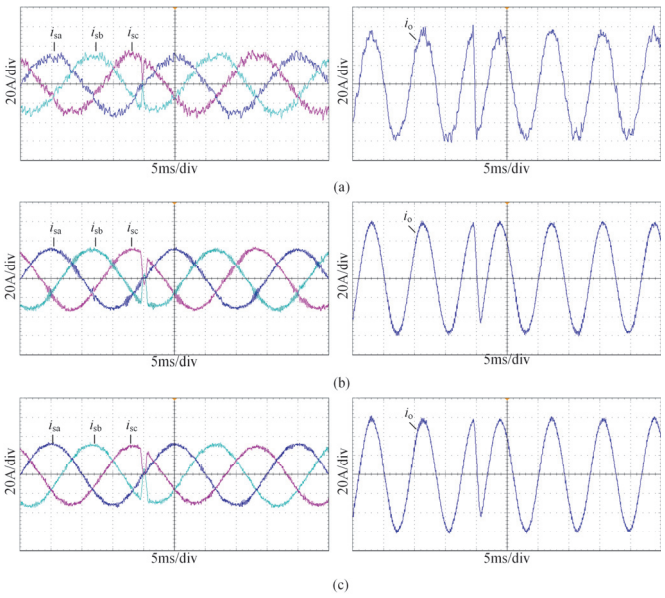

Fig. 14 Dynamic performance of input currents and output current with three different control methods. (a) Conventional MPC. (b) Proposed MMPC approach I. (c) Proposed MMPC approach II.

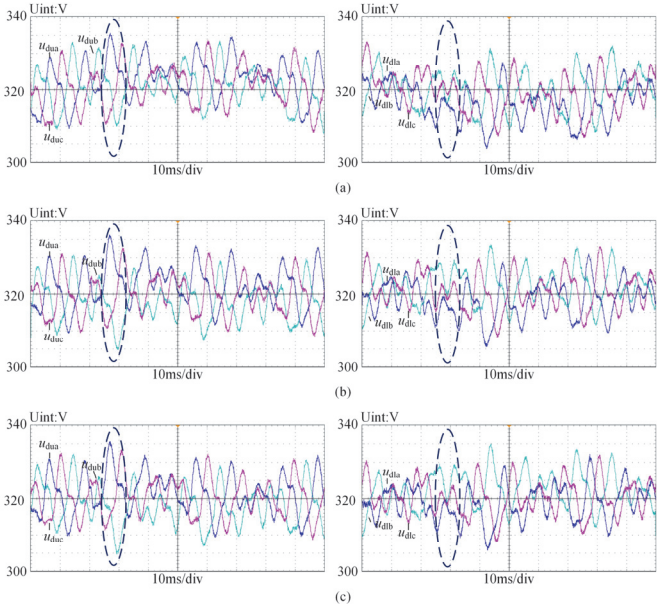

Fig. 15 Experimental waveforms of capacitor voltages during dynamic process. (a) Conventional MPC. (b) Proposed MMPC approach I. (c) Proposed MMPC approach II.

I and approach II show the similar dynamic performance. It worth mentioning that the two proposed MMPC methods maintain fast dynamic because the current tracking errors can be eliminated in a few control periods with these methods. Fig.15 shows the capacitor voltage of one SM in the upper and lower arm with these control methods, capacitor voltages are also kept steady during the dynamic transient.

VI. Conclusions

In this paper, multiple current tracking errors elimination is achieved at the end of each control period with the proposed MMPC methods. Level increment combinations are represented by vectors in the current increments plane for the first time. Eight sectors are defined according to the nine vectors along with the polarity and relationship of input current and circulating current tracking errors. In the proposed methods, modulated vectors sequence consisting of one zero vector and two active vectors with different duty cycles are utilized to eliminate these errors. Duty cycles are also derived for the zero vector and active vectors. The main difference between two proposed MMPC approaches is the selection of the optimal active vectors. Input current increment is limited more strictly in MMPC approach II. Steady state and dynamic performances of the proposed methods along with the conventional FCS-MPC method are evaluated. The results show that current tracking errors and current ripple are reduced simultaneously under the control of the proposed methods by introducing optimal vectors sequence with duty cycles, the MMPC approach I presents better output current performance while the MMPC approach II has lower input current ripples. The further investigation will focus on the improvement of the MPC considering parameter uncertainties, extending the adjacent level increments and the energy balancing control of MMC-ACPS operating around equal frequency.

References

[1] M. Glinka and R. Marquardt, "A New AC/AC Multilevel Converter Family," *IEEE Trans. Ind. Electron.*, vol. 52, no. 3, pp. 662-669, June. 2005.
[2] M. A. Perez, S. Bernet, J. Rodriguez, S. Kouro, and R. Lizana, "Circuit Topologies, Modeling, Control Schemes, and Applications of Modular Multilevel Converters," *IEEE Trans. Power Electron.*, vol. 30, no. 1, pp.

4-17, Jan. 2015.

[3] S. Debnath, J. C. Qin, B. Bahrani, M. Saeedifard, and P. Barbosa, "Operation, Control, and Applications of the Modular Multilevel Converter: A Review," *IEEE Trans. Power Electron*., vol. 30, no. 1, pp. 37-53, Jan. 2015.

[4] H. Akagi, "Classification, Terminology, and Application of the Modular Multilevel Cascade Converter (MMCC)," *IEEE Trans. Power Electron*., vol. 26, no. 11, pp. 3119-3130, Nov. 2011.

[5] A. Nami, J. Q. Liang, F. Dijkhuizen, and G. D. Demetriades, "Modular Multilevel Converters for HVDC Applications: Review on Converter Cells and Functionalities," *IEEE Trans. Power Electron*., vol. 30, no. 1, pp. 18-36, Jan. 2015.

[6] M. Vasiladiotis and A. Rufer, "Analysis and Control of Modular Multilevel Converters With Integrated Battery Energy Storage," *IEEE Trans. Ind. Electron*., vol. 30, no. 1, pp. 163-175, Oct. 2015.

[7] J. Kolb, F. Kammerer, M. Gommeringer, and M. Braun, "Cascaded Control System of the Modular Multilevel Converter for Feeding Variable-Speed Drives," *IEEE Trans. Power Electron*., vol. 30, no. 1, pp. 349-357, Jan. 2015.

[8] R. Darus, J. Pou, G. Konstantinou, S. Ceballos, R. Picas, and V. G. Agelidis, "A Modified Voltage Balancing Algorithm for the Modular Multilevel Converter: Evaluation for Staircase and Phase-Disposition PWM," *IEEE Trans. Power Electron*., vol. 30, no. 8, pp. 4119-4127, Aug. 2015

[9] M. Schnarrenberger, F. Kammerer, M. Gommeringer, J. Kolb, and M. Braun, "Current control and energy balancing of a square-wave powered 1AC-3AC modular multilevel converter," in *Proc. IEEE Energy Convers. Congr. Expo*., Sep. 2015, pp. 3607-3614.

[10] D. Karwatzki, M. Dokus, L. Baruschka, J. Kucka, and A. Mertens, "Branch energy balancing with a generalised control concept for modular multilevel topologies using the example of the modular multilevel converter," in *Proc. 18th Eur. Conf. Power Electron. Appl*., Sep. 2016, pp. 1-10.

[11] Johann W. Kolar, Thomas Friedli, Jose Rodriguez, and Patrick W. Wheeler, "Review of Three-Phase PWM AC–AC Converter Topologies," *IEEE Trans. Ind. Electron*., vol. 58, no. 11, pp. 4988-5006, Nov. 2011.

[12] F. Kammerer, J. Kolb, and M. Braun, "A novel cascaded vector control scheme for the modular multilevel matrix converter," in *Proc. 37th Annu. Conf. IEEE IECON*., Nov. 2011, pp. 1097-1102.

[13] L. Baruschka, and A. Mertens, "A New Three-Phase AC/AC Modular Multilevel Converter With Six Branches in Hexagonal Configuration," *IEEE Trans. Ind. Appl*., vol. 49, no. 3, pp. 1400-1410, Nov. 2013.

[14] Q. M. Xu, F. J. Ma, A. Luo, Y. D. Chen, and Z. X. He, "Hierarchical Direct Power Control of Modular Multilevel Converter for Tundish Heating," *IEEE Trans. Ind. Electron*., vol.63, no. 12, pp. 7919-7929, Dec. 2017.

[15] S. Li, X. Wang, Z. Yao, T. Li, and Z. Peng, "Circulating Current Suppressing Strategy for MMC-HVDC Based on Nonideal Proportional Resonant Controllers Under Unbalanced Grid Conditions," *IEEE Trans. Power Electron*., vol. 30, no. 1, pp. 387-397, Jan. 2015.

[16] Q. Tu, Z. Xu, and L. Xu, "Reduced Switching-Frequency Modulation and Circulating Current Suppression for Modular Multilevel Converters," *IEEE Trans. Power Del*., vol. 26, no. 3, pp. 2009-2017, Jul. 2011.

[17] M. Vasiladiotis, N. Cherix, and A. Rufer, "Accurate Capacitor Voltage Ripple Estimation and Current Control Considerations for Grid-Connected Modular Multilevel Converters," *IEEE Trans. Power Electron*., vol. 29, no. 9, pp. 4568-4579, Sep. 2014.

[18] X. J. Shi, B. Liu, Z. Q. Wang, Y. L. Li, L. M. Tolbert, and F. Wang, "Modeling, Control Design, and Analysis of a Startup Scheme for Modular Multilevel Converters," *IEEE Trans. Ind. Electron*., vol. 62, no. 11, pp. 7009-7024, Nov. 2015.

[19] L. Q. He, K. Zhang, J. Xiong, and S. F. Fan, "A Repetitive Control Scheme for Harmonic Suppression of Circulating Current in Modular Multilevel Converters," *IEEE Trans. Power Electron*., vol. 30, no. 1, pp. 471-481, 2015.

[20] S. Kouro, P. Cortés, R. Vargas, U. Ammann, and J. Rodríguez, "Model predictive control - a simple and powerful method to control power converters," *IEEE Trans. Ind. Electron*., vol. 56, no. 9, pp. 1826-1838, Jun. 2009.

[21] S. Vazquez, J. I. Leon, L. G. Franquelo, J. Rodriguez, H. A. Young, A. Marquez, and P. Zanchetta., "Model Predictive Control: A Review of Its Applications in Power Electronics," *IEEE Trans. Ind. Electron. Mag*., vol. 8, no. 1, pp. 16-31, Mar. 2014.

[22] C. Bordons and C. Montero, "Basic Principles of MPC for Power Converters: Bridging the Gap Between Theory and Practice," *IEEE Trans. Ind. Electron. Mag*., vol. 9, no. 3, pp. 31-43, Sept. 2015.

[23] S. Vazquez, J. Rodriguez, M. Rivera, L. G. Franquelo, and M. Norambuena, "Model Predictive Control for Power Converters and Drives: Advances and Trends," *IEEE Trans. Ind. Electron.*, vol. 64, no. 2, pp. 935-947, Feb. 2017.

[24] Zhang Y C, Xie W, and Li Z X, "Model predictive direct power control of a PWM rectifier with duty cycle optimization," *IEEE Trans. Power Electron*., vol. 28, no. 11, pp. 5343-5351, 2013.

[25] Qin Q C, and Saeedifard M, "Predictive control of a modular multilevel converter for a back-to-back HVDC system," *IEEE Trans. Power Del*., vol. 27, no. 3, pp. 1538-1547, Jul. 2012.

[26] L. Ben-Brahim, A. Gastli, M. Trabelsi, K. A. Ghazi, M. Houchati, and H. Abu-Rub, "Modular Multilevel Converter Circulating Current Reduction Using Model Predictive Control," *IEEE Trans. Ind. Electron.*, vol. 63, no. 6, pp. 3857-3866, Jun. 2016.

[27] B. S. Riar, T. Geyer, and U. K. Madawala, "Model Predictive Direct Current Control of Modular Multilevel Converters: Modeling, Analysis, and Experimental Evaluation," *IEEE Trans. Power Electron*., vol. 30, no. 1, pp. 431-439, Jan. 2015.

[28] J. Böcker, B. Freudenberg, A. The, and S. Dieckerhoff, "Experimental Comparison of Model Predictive Control and Cascaded Control of the Modular Multilevel Converter," *IEEE Trans. Power Electron*., vol. 30, no. 1, pp. 422-430, Jan. 2015.

[29] M. A. Perez, J. Rodriguez, E. J. Fuentes, and F. Kammerer, "Predictive Control of AC–AC Modular Multilevel Converters," *IEEE Trans. Ind. Electron.*, vol. 59, no. 7, pp. 2832-2839, Jul. 2012.

[30] J. W. Moon, J. S. Gwon, J. W. Park, D. W. Kang, and J. M. Kim, "Model Predictive Control With a Reduced Number of Considered States in a Modular Multilevel Converter for HVDC System," *IEEE Trans. Power Del*., vol. 30, no. 2, pp. 608 - 617, Jan. 2015.

[31] Vatani M, Bahrani B, and Saeedifard M, "Indirect finite control set model predictive control of modular multilevel converters," *IEEE Trans. Smart Grid*, vol. 6, no. 3, pp. 1520-1529, May. 2015.

[32] A. Dekka, B. Wu, V. Yaramasu, and N. R. Zargari, "Dual-Stage Model Predictive Control With Improved Harmonic Performance for Modular Multilevel Converter," *IEEE Trans. Ind. Electron.*, vol. 63, no. 10, pp. 6010-6019, Oct. 2016.

[33] A. Rashwan, M. A. Sayed, Y. Mobarak, G. Shabib, and T. Senjyu, "Predictive Controller Based on Switching State Grouping for a Modular Multilevel Converter with Reduced Computational Time," *IEEE Trans. Power Del*., vol. PP, no. 99, pp. 1-1, 2016.

[34] F. Zhang, W. Li, and G. Joós, "A Voltage-Level-Based Model Predictive Control of Modular Multilevel Converter," *IEEE Trans. Ind. Electron.*, vol. 63, no. 8, pp. 5301-5312, Aug. 2016.

[35] Z. Gong, P. Dai, X. B. Yuan, X. J. Wu, and G. S. Guo, "Design and Experimental Evaluation of Fast Model Predictive Control for Modular Multilevel Converters," *IEEE Trans. Ind. Electron*., vol. 63, no. 6, pp. 3845-3856, Jun. 2016.

[36] Sangshin Kwak, Soo-Eon Kim, and Jun-Cheol Park, "Predictive Current Control Methods With Reduced Current Errors and Ripples for Single-Phase Voltage Source Inverters," *IEEE Trans. Ind. Informat.*, vol. 11, no. 5, pp. 1006-1016, Oct. 2015.

[37] Y. C. Zhang, W. Xie, Z. X. Li, and Y. C. Zhang, "Low-Complexity Model Predictive Power Control: Double-Vector-Based Approach," *IEEE Trans. Ind. Electron*., vol. 61, no. 11, pp. 5871-5880, Nov. 2014.

[38] F. J. Ma, Z. X. He, Q. M. Xu, A. Luo, L. M. Zhou, and M. S Li, "Multilevel Power Conditioner and its Model Predictive Control for Railway Traction System," *IEEE Trans. Ind. Electron*., vol.63, no. 11, pp. 7275-7285, Nov. 2016.

[39] L. Tarisciotti, P. Zanchetta, A. Watson, S. Bifaretti, and J. C. Clare, "Modulated Model Predictive Control for a Seven-Level Cascaded H-Bridge Back-to-Back Converter," *IEEE Trans. Ind. Electron*., vol.61, no. 10, pp. 5375-5383, Oct. 2014.

[40] Hamid Mahmoudi, Mohsen Aleenejad, and Reza Ahmadi, "Modulated Model Predictive Control of Modular Multilevel Converters in VSC-HVDC Systems," *IEEE Trans. Power. Delivery*., vol. PP, no. 99, pp. 1-1. 2018.

[41] H. Fujita, S. Tominaga, and H. Akagi, "Analysis and design of a dc voltage-controlled static var compensator using quad-series voltage source inverters," *IEEE Trans. Ind. Appl*., vol. 32, no. 4, pp. 970–977, Jul./Aug. 1996.

This article has been accepted for publication in a future issue of this journal, but has not been fully edited. Content may change prior to final publication. Citation information: DOI 10.1109/TPEL.2019.2895224, IEEE Transactions on Power Electronics

Zhixing He (S'15- M'17) was born in Hunan, China, 1989. He received the B.S. degree in information science and Engineering from Central South University, Changsha, China, in 2011, and the Ph.D. degree in electrical engineering from Hunan University, Changsha, China, in 2017. He was with the Hunan University, as postdoctoral researcher between 2017 and 2018. Currently, he has been an Associate Professor in the College of Electrical and Information Engineering, Hunan University, Changsha, China. His research interests include power electronics, medium voltage dc system, model predictive control and modular multilevel converter.

Peng Guo (S'18) was born in Hunan, China, in 1992. He received the B.S. degree in electrical engineering from the Wuhan University of Technology, Wuhan, China, in 2015, and is currently working toward Ph.D. degree in Electrical Engineering in the College of Electrical and Information Engineering, Hunan University, Changsha.
His main research interests include modular multilevel converter, model predictive control and its applications in power electronics.

Zhikang Shuai (S'09-M'10-SM'17) received the B.S. and Ph.D. degree from the College of Electrical and Information Engineering, Hunan University, Changsha, China, in 2005 and 2011, respectively, all in electrical engineering. He was with the Hunan University, as an Assistant Professor between 2009 and 2012, and an Associate Professor in 2013. Starting in 2014, he became a Professor at Hunan University. His research interests include power quality control, power electronics, and Microgrid stability analysis and control. Dr. Shuai is the Associate Editor of IEEE Journal of Emerging and Selected Topics in Power Electronics, Chinese Journal of Electrical Engineering. He is a recipient of the 2010 National Scientific and Technological Awards of China, the 2012 Hunan Technological Invention Awards of China, the 2007 Scientific and Technological Awards from the National Mechanical Industry Association of China.

Qianming Xu (M'17) was born in Henan, China, in 1989. He received the B.S. degree in electrical engineering and automation and the Ph.D. degree in electrical engineering from Hunan University, Changsha, China, in 2012 and 2017, respectively.
Since 2017, he has been an Assistant Professor in the College of Electrical and Information Engineering, Hunan University.
His research interests include modular multilevel converter, power quality control, and dc grid control.

An Luo (SM'09) was born in Changsha, China, in 1957. He received the B.S. and M.S. degrees in industrial automation from Hunan University, Changsha, in 1982 and 1986, respectively, and the Ph.D. degree in fluid power transmission and control from Zhejiang University, Hangzhou, China, in 1993. Between 1996 and 2002, he was a Professor with Central South University.
Since 2003, he has been a Professor in the College of Electrical and Information Engineering, Hunan University, where he also serves as the Chief of National Electric Power Conversion and Control Engineering Technology Research Center.
His research interests mainly include distributed generation, microgrid, and power quality. He was elected to the Chinese National Academy of Engineering (CNAE) in 2015, the highest honor for scientists and engineers and scientists in China. He has won the highly prestigious China National Science and Technology Awards three times (2014, 2010 and 2006).

Josep M. Guerrero (S'01-M'04-SM'08-FM'15) received the B.S. degree in telecommunications engineering, the M.S. degree in electronics engineering, and the Ph.D. degree in power electronics from the Technical University of Catalonia, Barcelona, in 1997, 2000 and 2003, respectively. Since 2011, he has been a Full Professor with the Department of Energy Technology, Aalborg University, Denmark. From 2015 he is a distinguished guest Professor in Hunan University.
His research interests mainly include power electronics, distributed energy-storage, and microgrids. Prof. Guerrero is an Associate Editor for the IEEE TRANSACTIONS ON POWER ELECTRONICS, the IEEE TRANSACTIONS ON INDUSTRIAL ELECTRONICS, and the IEEE Industrial Electronics Magazine, and an Editor for the IEEE TRANSACTIONS on SMART GRID and IEEE TRANSACTIONS on ENERGY CONVERSION. In 2014, 2015, and 2016 he was awarded by Thomson Reuters as Highly Cited Researcher, and in 2015 he was elevated as IEEE Fellow for his contributions on distributed power systems and microgrids.